PHYSICAL REVIEW B, VOLUME 65, 214424

Critical behavior of $La_{0.75}Sr_{0.25}MnO_3$

D. Kim, B. L. Zink, and F. Hellman
Department of Physics, University of California, San Diego, La Jolla, California 92093

J. M. D. Coey
Physics Department, Trinity College, Dublin 2, Ireland

(Received 17 November 2000; published 7 June 2002)

Magnetization, susceptibility, and specific heat measurements were made on a single crystal of $La_{0.75}Sr_{0.25}MnO_3$. The ferromagnetic-to-paramagnetic phase transition was found at 346 K and four critical exponents were measured as: $\alpha = 0.05 \pm 0.07$, $\beta = 0.40 \pm 0.02$, $\gamma = 1.27 \pm 0.06$, and $\delta = 4.12 \pm 0.33$. The values of critical exponents are all between mean-field values and three-dimensional-(3D)-Ising-model values. The scaling behavior is well obeyed for all measurements, and the associated exponent relations are well satisfied, validating the critical analysis. Although the cubic crystal structure of this material makes the 3D Heisenberg the expected model, uniaxial magnetic anisotropy arising from the shape of the sample causes the 3D Ising model to be important within the experimental temperature range.

DOI: 10.1103/PhysRevB.65.214424 PACS number(s): 75.40.Cx, 75.30.Vn, 64.60.Fr

I. INTRODUCTION

Interest in the perovskite manganites $A_{1-x}B_xMnO_3$ (A, trivalent rare earth; B, divalent metal) has revived since the discovery[1] of colossal magnetoresistance (CMR) near the Curie temperature T_C for x near 0.3. Some manganites are also believed to possess strongly spin-split bands, leading to what is called half-metallicity (complete spin polarization of the charge carriers at the Fermi level). The magnetotransport behavior and the possibility of applications utilizing CMR or half-metallicity motivated intensive studies on the underlying physics.[2,3] Above T_C, CMR perovskite manganites are paramagnetic insulators (insulating in the sense that the temperature dependence of the resistivity $d\rho/dT<0$). As the temperature is decreased below T_C, they become ferromagnetic metals. Among the perovskite manganites, $La_{1-x}Sr_xMnO_3$ (LSMO) has the highest $T_C \sim 370\,K$. Replacement of La by Pr, Nd, and Sm or of Sr by Ca, Ba, and Pb results in distortions of MnO_6 octahedra in the pseudocubic structure (hence increased electron-phonon coupling), lower T_C, and higher resistivity by several orders of magnitude.[4] The lower-T_C materials are reported to exhibit phase separation of metallic and insulating regions below T_C,[5] leading to a possible first-order phase transition at T_C.[6] $La_{1-x}Sr_xMnO_3$ however is the most metallic in the manganite family and therefore has the most itinerant electrons. There is a report of phase separation on the surface of LSMO by scanning-tunnel-microscope experiment, but other bulk experiments indicate no phase separation.[7]

For a second-order phase transition near the critical temperature, where a correlation length can be defined, the specific heat, spontaneous magnetization $[M_S \equiv M(H=0)]$, and initial magnetic susceptibility $(\chi \equiv \partial M/\partial H|_{H=0})$ show power-law dependence on the reduced temperature, $t \equiv (T-T_C)/T_C$. Also at T_C, M has a power-law dependence on H,

$$C_+(T) \sim A|t|^{-\alpha}/\alpha, \quad t>0,$$

$$C_-(T) \sim A'|t|^{-\alpha'}/\alpha', \quad t<0,$$

$$M_S(T) \sim B|t|^{\beta}, \quad t<0,$$

$$\chi(T) \sim C|t|^{-\gamma}, \quad t>0,$$

$$M(H) \sim DH^{1/\delta}, \quad t=0.$$

Here A, A', B, C, and D are constants. Scaling requires that $\alpha=\alpha'$. In addition, there are two exponent relations that limit the number of independent variables to two,

$$\alpha + 2\beta + \gamma = 2,$$

$$\gamma = \beta(\delta - 1).$$

Separate studies of magnetization and specific heat critical phenomena have been reported, both on single crystals and on polycrystalline samples.[3,8–10] These have indicated inconsistent results, with magnetization critical exponents varying fairly widely. For characterization of critical phenomena, high-quality samples with a large grain size and preferably a single crystal are needed to avoid smearing of T_C. For epitaxial thin-film samples, the small signal makes it hard to get data of the quality needed for critical analysis, given the signal-to-noise ratio. Also as T gets near T_C, the correlation length can be of the order of the thickness of the sample, thus switching from three-dimensional (3D) to 2D behavior. A single crystal of $La_{0.7}Sr_{0.3}MnO_3$ was measured by Ghosh *et al.*, who found $\beta = 0.37 \pm 0.04$, $\gamma = 1.22 \pm 0.03$, and $\delta = 4.25 \pm 0.2$, fit with a reduced temperature t range of 0.002 to 0.03.[3] Mohan *et al.* measured a polycrystalline sample of $La_{0.8}Sr_{0.2}MnO_3$ and found significantly different values: $\beta = 0.50 \pm 0.02$, $\gamma = 1.08 \pm 0.03$, and $\delta = 3.13 \pm 0.2$ (all much closer to mean-field values) with $|t|<0.008$.[9] It is not clear if the differences reflect the polycrystalline nature, the different composition, or the different t range. Neutron-scattering studies on a single crystal of $La_{0.7}Sr_{0.3}MnO_3$ yielded a value of $\beta=0.295$ but the t range used was somewhat far from the transition.[10] Lin *et al.* measured magnetization exponents of $La_{0.7}Sr_{0.3}MnO_3$ and found $\beta=0.31$ and $\delta=5.1$, fit in a non-specified t range, and a specific heat critical exponent α, which is anomalously large $(+0.16)$ and inconsistent with their magnetization data.[8] For these reasons, we report here a study of the specific heat, magnetic susceptibility, and spontaneous magnetization on a single sample of single crystal $La_{0.75}Sr_{0.25}MnO_3$ very near T_C.

II. EXPERIMENT

A. Specific-heat measurement

Single crystal $La_{0.75}Sr_{0.25}MnO_3$ was made by a floating-zone process. Viret *et al.* previously made small-angle, polarized neutron-scattering measurements[11] on a sample from the same batch. The sample used in the specific heat measurement is a thin flake of approximate dimensions $0.2\times0.5\times0.5\,\mathrm{mm}^3$, weighing 212 μg. To make this measurement, we used a microcalorimeter originally developed by our group to measure the specific heat of thin films of thickness 200–400 nm weighing 2–20 μg.[12] For this experiment, we modified the design of the microcalorimeter to allow us to measure a bulk sample attached by indium. The modified calorimetry device consists of a 1.5-μm-thick amorphous silicon-nitride membrane of $5\times5\,\mathrm{mm}^2$ lateral size. The central 2.5×2.5-mm^2 sample area is covered by a 1.5-μm-thick evaporated gold film, which has high thermal conductivity. Indium was used to thermally and physically attach the sample to the gold layer. Due to the high thermal conductivity of the gold layer and the poor thermal conductivity of the amorphous SiN membrane, the sample area is linked to the Si frame only by a very weak thermal link and is effectively isothermal on the experimental time scale. On the front side of the membrane, platinum thermometers and heaters were evaporated and patterned by photolithography. The relaxation method was used to measure the heat capacity. Reference 12 describes the experiment in more detail.

Figure 1 shows a schematic of the series of experiments performed to measure the specific heat C_P of the single crystal $La_{0.75}Sr_{0.25}MnO_3$. Figures 1(a)–1(c) are side views of the micro-calorimetry device in three different stages of the experiment. Fig. 1(a) shows the C_P1 measurement; this includes the heat capacity of the Au layer, the Pt heater and thermometer, and the silicon-nitride membrane. Seventy-two micrograms of In is then bonded to the gold layer, using a hot plate to melt In, after which C_P2 was measured as shown in Fig. 1(b). The heat capacity of the 72 μg of In was determined by subtracting C_P1 from C_P2. The single-crystal manganite sample did not stick well to the In (even above the In melting temperature) without applying pressure, which has a danger of breaking the SiN membrane. Instead we pressed the sample into an additional 96 μg of In. This sample/In piece can then be attached easily to the existing In on the device, once again using a hot plate. Figure 1(c) shows the device with additional In and bulk sample, measured as C_P3. Subtracting C_P2 from C_P3 yields the heat capacity of 96 μg of In and 212 μg of $La_{0.75}Sr_{0.25}MnO_3$. Since we have already measured the specific heat of In in C_P2, the heat capacity of 96 μg of In can be subtracted, yielding the heat capacity of $La_{0.75}Sr_{0.25}MnO_3$.

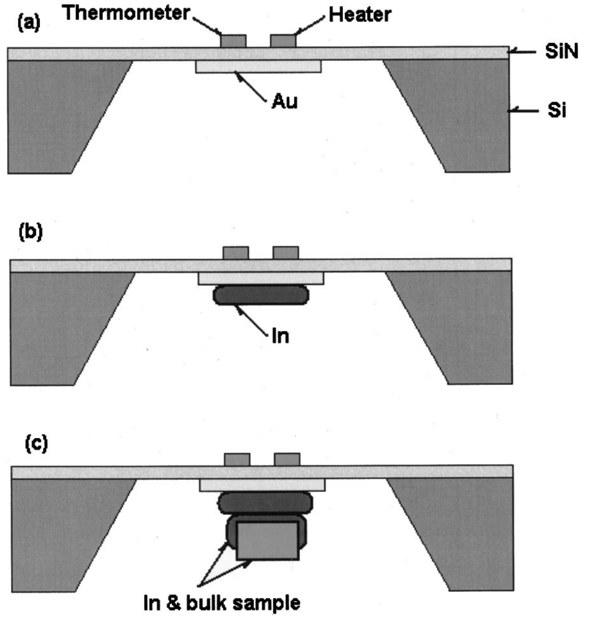

FIG. 1. Side view of microcalorimetry device and sample showing steps used to measure $C_P(T)$. (a) Measure C_P1; includes Au conduction layer, Pt heater and thermometer, and SiN membrane. (b) Measure C_P2 after attaching 72 μg of In. C_P2-C_P1 $=$heat capacity of 72-μg In. (c) Measure C_P3 after attaching another 96 μg of In and 212 μg of $La_{0.75}Sr_{0.25}MnO_3$. C_P3-C_P2 $=$heat capacity of 96 μg of In$+$212 μg of $La_{0.75}Sr_{0.25}MnO_3$. Subtraction of In contribution $[=96/72^*(C_P2-C_P1)]$ gives C_P of $La_{0.75}Sr_{0.25}MnO_3$

B. Magnetization measurements

Another thin flake ($0.2\times0.7\times0.8\,\mathrm{mm}^3$; 750 μg) of single crystal $La_{0.75}Sr_{0.25}MnO_3$, grown and cut from the same batch as the sample used in the specific heat experiment, was used for magnetization measurements. Room-temperature torque magnetometry was first used to characterize the magnetic anisotropy. Shape anisotropy was found to dominate the intrinsic cubic anisotropy. The sample has an easy plane of magnetization (perpendicular hard axis with $K_H=5.1\times10^5\,\mathrm{dyne/cm}^2$), and within the plane, the easy axis is along the longest body diagonal of the slightly rhombic shape ($K_E=8.1\times10^4\,\mathrm{dyne/cm}^2$).

A Quantum Design dc superconducting quantum interference device magnetometer was used to measure the magnetization. All measurements were made with the magnetic field applied along the easy axis. Figure 2 shows the magnetization versus applied field $[M(H_a)]$ curves at different temperatures. At very low temperatures, the saturated magnetization reached the expected spin-only magnetization of $3.75\mu_B/\mathrm{Mn}$ atom. The reduction of magnetization due to spin canting reported elsewhere for a polycrystalline sample[13] was not observed. The coercivity is very low (less

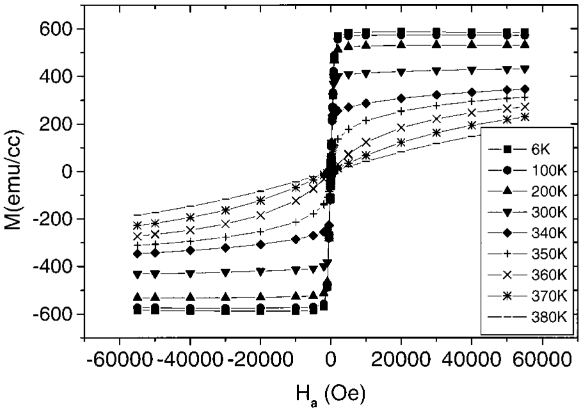

FIG. 2. M vs H_a hysteresis curves along the easy axis at different temperatures. Low-field susceptibility gives demagnetization factor D, due to small shape anisotropy of slab-shaped sample.

than 10 Oe) and no hysteresis was observed at fields >100 Oe, most likely due to the sample quality and single-crystal nature. The steep rise in M near $H_a = 0$ is due to domain-wall movement. $M(H_a)$ is linear until M is very near the spontaneous magnetization M_S for each temperature. From the slope of the $M(H_a)$ curve near zero field, the demagnetization factor D was calculated, $D = H_a/M$. The demagnetization field $H_D = DM$ is small compared to the high applied fields (less than 4% at 10 000 Oe), and becomes more significant at low applied fields reaching 50% around 400 Oe. In order to minimize the error arising from the determination of D, only data with H_D less than 50% of H_a were used in the critical analysis below. Throughout this article, H_a stands for the applied field and $H = H_a - H_D = H_a - DM$ is the corrected magnetic field after subtraction of the demagnetization field.

III. RESULTS

A. Specific heat

Figure 3 shows the specific heat of $La_{0.75}Sr_{0.25}MnO_3$ between 80 and 430 K. Above the transition temperature, the absolute value of the specific heat is just above the Dulong-Petit limit, 125 J/mol K 1 mole of $La_{0.75}Sr_{0.25}MnO_3$ weighs 229 g and has one acoustic mode and four optical modes per formula unit. Since the phonon contribution is dominant at this high temperature, almost all phonon modes must be excited to account for this large value of the specific heat, i.e., Debye and Einstein temperatures less than 400 K. In addition to the phonon contribution, there will be an electronic specific heat $\gamma T \sim 3\,\mathrm{J\,K^{1}\,mol^{-1}}$ and a positive dilation term, $(C_P - C_V) \sim 0.4\,\mathrm{J\,K^{-1}\,mol^{-1}}$, due to the expansion of the sample. These two contributions are less than 3% of the total C_P, based on low-temperature determinations of $\gamma \sim 3-6\,\mathrm{mJ\,K^{-2}\,mol^{-1}}$ (Refs. 4 and 14) and estimates of $(C_P - C_V)$ from thermal-expansion measurements of LSMO (Ref. 15) and bulk modulus of $La_{1.8}Sr_{0.2}CuO_4$.[16,17]

The most obvious feature in $C_P(T)$ is the λ-shaped peak located near 347 K associated with the phase transition. The sharpness of the peak indicates the uniformity and homogeneity of this single-crystal sample. After an initial specific heat measurement to locate the peak temperature, we varied the temperature near the peak by small amounts to get many data points near the critical temperature to do scaling analysis. $C_P(T)$ near T_C is composed of a smooth background plus a singular part, C_S, due to the magnetic phase transition. The smooth background comes primarily from phonons and free electrons, but can also include a non-singular contribution to the magnetic specific heat. As is commonly done, we assumed that this background in the small region near T_C between 321 and 354 K is linear in temperature. We used the least-squares method to fit $C_P(T)$ data. Following the method of Kornblit and Ahlers,[18] the functions we used to fit $C_P(T)$ in this region are

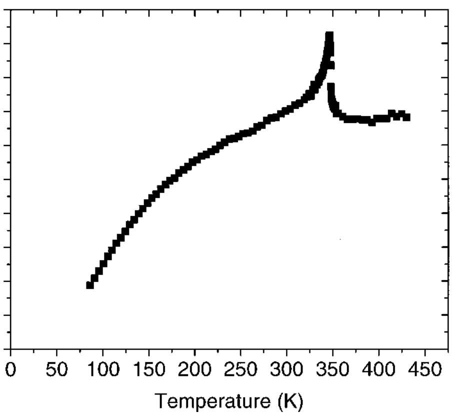

FIG. 3. Specific heat of $La_{0.75}Sr_{0.25}MnO_3$ obtained following procedure outlined in Fig. 1. Sample mass was 212 μg. 1 mole weighs 229 g. Heat capacity of the sample was of the order of 50% of the total measured heat capacity C_P3.

$$C_P^+(t) = (A/\alpha)|t|^{-\alpha} + B + Ct \quad \text{for } t>0,$$

$$C_P^-(t) = (A'/\alpha)|t|^{-\alpha} + B + Ct \quad \text{for } t<0.$$

Here C represents the slope of the underlying physical smooth background. C has to be the same above and below T_C because the smooth background should not have a discontinuous derivative at T_C. B consists of the specific heat of the underlying smooth background at T_C (B_1) plus a constant B_2. B_2 is used to fit the critical region in conjunction with a simple power-law term.[18] Therefore, $B = B_1 + B_2$. $B_1 + C\,t$ is the physical smooth background containing the noncritical contributions of phonons, electrons, and magnetic excitations. The alternative approach, which is often used, is to fit the physical smooth background through T_C using the measured $C_P(T)$ far from T_C or using high fields to suppress the fluctuations. In this case, a different form for C_P^+ and C_P^- is used. The merits of these two approaches have been discussed by Kornblit and Ahlers.[18] It is certain that the same value of B_1 should be used for both above and below T_C, because the smooth background has to be continuous at T_C. If we assume the continuity of total specific heat $C_P(T)$ at the critical temperature when $\alpha < 0$ (cusp), then the same value of B_2 (hence the same value of B) above and below T_C is necessary. Note that in the case of $\alpha < 0$, B is larger than

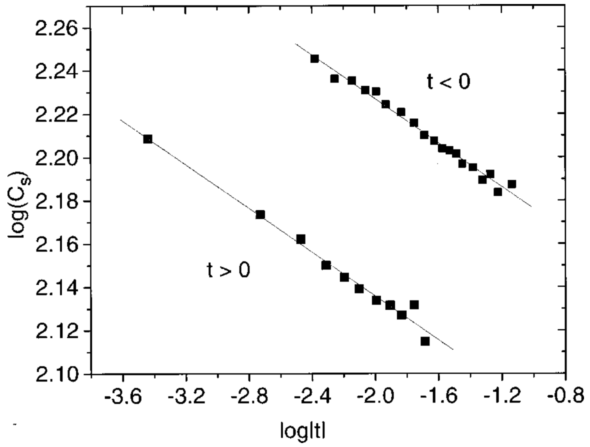

FIG. 4. $\log_{10}(C_S)$ vs $\log_{10}(|t|)$ fit for both $t<0$ and $t>0$. $\alpha(t>0)=\alpha'(t<0)=0.05$. The slope is $-\alpha$.

$C_P(T)$, and $B+C\,t$ lies above the specific heat curve although of course $B_1+C\,t$ lies below. Whether B_2 is continuous for $\alpha>0$ is not as obvious. Kornblit and Alhers discussed this issue in their work and chose to constrain it to be continuous.[18] We have followed this method and also have constrained it to be continuous. We assumed $\alpha(t>0)=\alpha'(t>0)$, adopting scaling theory. B and C were then varied over a wide range and we adjusted T_C for each set of parameters (B, C) to satisfy $\alpha=\alpha'$. We defined χ^2 as

$$\chi^2=\sum_{t_i>0}\frac{[C_P-\{(A/\alpha)|t_i|^{-\alpha}+B+Ct_i\}]^2}{(0.005C_P^2)}+\sum_{t_i=0}\frac{[C_P-\{(A'/\alpha')|t_i|^{-\alpha'}+B+Ct_i\}]^2}{(0.005C_P^2)},$$

where t_i denotes each experimental reduced temperature. χ^2 is a measure of the quality of the fit. In calculating χ^2, each data point had a weight of $1/(0.005C_P)^2$, where we estimated 0.5% error in $C_P(T)$ data. Absolute accuracy in C_P is estimated to be ±2%, dominated by uncertainty in the addenda subtraction and in the absolute temperature scale of the commercially calibrated thermometers. Relative precision is estimated at 0.5% and is dominated by noise. We used the grid-search method[19] to get the best fit with the lowest χ^2. The parameters with the best fit were $B=5.26$, $C=147.55$, and $T_C=347.22$ K. Assuming the smooth physically relevant background $B_1\sim130$ from Fig. 3, $B_2=B-B_1\sim-125$. The value of C is large compared to the expected background slope of ~50. Forcing the background to fit the apparent slope of 50 changes α to 0.06 with a slightly worse fit; this value of α is within the range we find below for α, hence the difference is not significant.

Defining the singular part of the specific heat,

$$C_S(t)=C_P(t)-(B+Ct)=(A/\alpha)|t|^{-\alpha},$$

$\log_{10}C_S$ vs $\log_{10}|t|$ will yield two straight lines for $t<0$ and $t>0$ with the slope of $-\alpha$. Figure 4 shows the log-log plot with the parameters mentioned above. The critical exponent α was 0.05. χ^2 contour plots were used to determine the range of α within the two standard-deviation contour for 95% confidence levels. From this, the range of α was determined as $(-0.022, 0.11)$. The reduced temperature range for this determination is $-7.3\times10^{-2}<t<-3.6\times10^{-4}$.

The amplitude ratio A/A' is also a universal quantity with large variation between different universality classes. The value 0.81 in Table I is the result of the best fit described above. The range of A/A' is obtained using the same two standard-deviation contour for χ^2. The values for A/A' (and the error bars) are anticorrelated to the values of α, e.g., for $\alpha=-0.022$, $A/A'=1.1$ and for $\alpha=+0.12$, $A/A'=0.63$.

B. Magnetization

We used a modified Arrot plot scheme to determine the critical exponents β and δ, as reviewed by Kaul.[20] The scaling equation of state

$$(H/M)^{1/\gamma}=at+bM^{1/\beta}$$

causes isothermal curves of $M(H)$ data to fall into a set of parallel straight lines in a plot of $M^{1/\beta}$ vs $(H/M)^{1/\gamma}$ if the correct values of β and γ are chosen. For the mean-field values of $\beta=0.5$ and $\gamma=1$, this is the well-known Arrot-Kouvel plot, but departures from mean-field values necessitate the use of this modified Arrot plot. Note that the intercepts of the isotherms on the x and y axes are $(1/\chi)^{1/\gamma}$ for $t>0$ and $M_S^{1/\beta}$ for $t>0$, respectively. The isothermal line that passes through the origin is the critical isotherm at $T=T_C$. To find the correct values of β and γ, an initial choice of β and γ is made, yielding quasi-straight lines in the modified Arrot plot. From these initial values of β and γ, linear fits to the isotherms are made to get the intercepts giving $M_S(T)$ and $\chi(T)$, and an initial value of T_C was determined from the isotherm that passes through the origin. From these

TABLE I. Comparison of measured critical exponents with different theoretical models.

	α	β	γ	δ	A/A'
This work	0.05 ± 0.07	0.40 ± 0.02	1.27 ± 0.06	4.12 ± 0.33	$0.81\mp0.18/0.29$[a]
t range (this work)	(0.000 36, 0.073)	(0.000 006, 0.0004)	(0.0006, 0.006)	N/A	
MF theory	0 (discontinuity)	0.5	1.0	3.0	
3D Ising model	0.11	0.325	1.24	4.82	0.524
3D *XY* model	−0.007	0.333	1.34		1.03
3D Heisenberg model	−0.115	0.365	1.336	4.80	1.521

[a] Values for α and A/A' are correlated. $A/A'=0.63$ when $\alpha=0.12$; $A/A'=1.1$ when $\alpha=-0.022$.

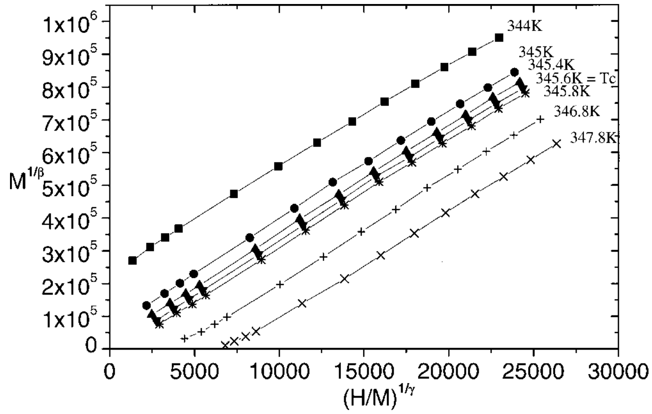

FIG. 5. Modified Arrot plot after 30 iterations for the convergence of β and γ. Isothermal curves fall into a set of parallel straight lines. Intercepts give $M_S(T)$ and $1/\chi(T)$.

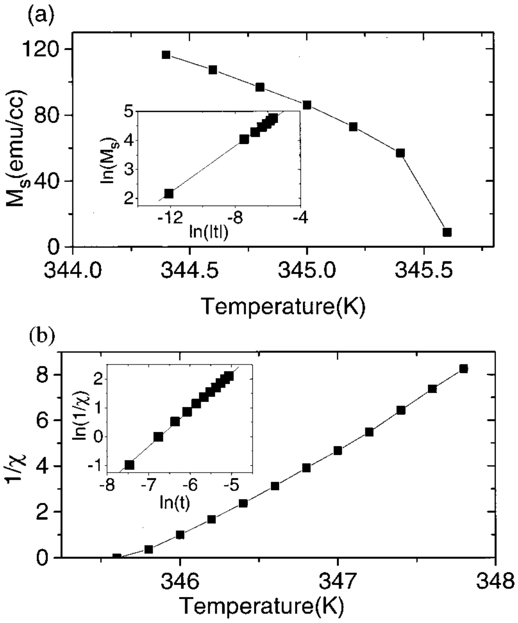

FIG. 6. (a) M_S vs T, obtained from X intercepts of Fig. 5. Inset shows ln(M_S) vs ln($|t|$); slope gives $\beta = 0.40 \pm 0.02$. (b) $1/\chi$ vs T, obtained from Y intercepts of Fig. 5. Inset shows ln($1/\chi$) vs ln($|t|$); slope gives $\gamma = 1.27 \pm 0.06$.

$M_S(t)$ data, a new value of β is obtained from a $\ln[M_S(t)]$ vs $\ln(|t|)$ plot by fitting the data to a straight line, the slope of which is $1/\beta$. Similarly a new value of γ is obtained from the $\ln(1/\chi)$ vs $\ln(t)$ plot. These new values of β and γ are then used to make a new modified Arrot plot. From this new modified Arrot plot, improved values of T_C, $M_S(T)$, and $\chi(T)$ are obtained, yielding better values of β and γ. By iterating this method, the values of T_C, β, and γ converged to stable values. Figure 5 is the final result of these iterations for 400 Oe$<H_a<$10 000 Oe. As previously discussed, fields below 400 Oe were not included because the uncertainty in the demagnetization correction becomes large. The isotherms in Fig. 5 are quite parallel with slopes within 1% of each other. T_C was determined from Fig. 5 to be 345.6 K by finding the isotherm passing through the origin. This value of T_C differs by ~1.5 K (<0.5%) from the value obtained from specific-heat measurement, due most likely to slightly different thermometer calibrations for each experimental setup since the absolute value of commercial thermometers is not calibrated better than 1%. (The relative values of temperature, required for the critical analysis, are however far better than 1%.) From the x and y intercepts of Fig. 5, $M_S(T)$ and $1/\chi(T)$ were obtained as shown in Figs. 6(a) and 6(b). The insets show the ln-ln plots used to get the final values of β and γ. Error bars come from the deviation of the least-squares fit analysis. The value of $\beta = 0.40 \pm 0.02$ is near the 3D Heisenberg ferromagnet value of 0.37. The value of $\gamma = 1.27 \pm 0.06$ is near but smaller than the 3D Heisenberg value 1.39. The reduced-temperature range used for these fits is 6×10^{-4}–$6\times10^{-3}(t>0)$ and 6×10^{-6}–$4\times10^{-3}(t<0)$.

The $M(H)$ curve at the critical temperature, $T_C = 345.6$ K, is plotted in Fig. 7. From the ln-ln plot shown in the inset, the critical exponent $\delta = 4.12$, significantly smaller than the 3D Heisenberg value of 4.8 but larger than the mean-field value of 3.0. δ determined from neighboring temperatures, 345.4 and 345.8 K, were 4.09 and 4.45, respectively. From this the error of δ was set as $\delta = 4.12 \pm 0.33$.

As a further test, the static-scaling hypothesis predicts that $M(t,H)$ is a universal function of t and H,

$$M(t,H)/t^{\beta} = f_{\pm}[H/t^{(\beta+\gamma)}],$$

where f_+ is for $t>0$, and f_- is for $t<0$. By plotting M/t^{β} vs $H/t^{(\beta+\gamma)}$, all data points below T_C are expected to fall on f_-, whereas the data points above T_C will be on f_+. Figure 8 shows such a scaling plot both on a linear scale, which emphasizes the high-field data and on a log scale, which emphasizes the low-field data. Indeed all data points over the entire range of the variables fall on two branches of curves depending on the sign of t.

Finally, the two predicted exponent relations were checked. $\alpha + 2\beta + \gamma = 2$ (theory), 2.12 ± 0.13 (experiment) is

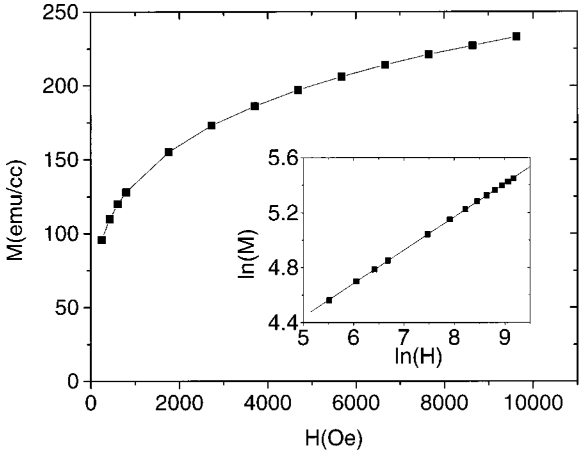

FIG. 7. Critical isothermal curve of $M(H)$, taken from Fig. 5 zero intercept, which gives T_C. Inset shows ln(M) vs ln(H) plot at T_C; slope gives $\delta = 4.12 \pm 0.2$.

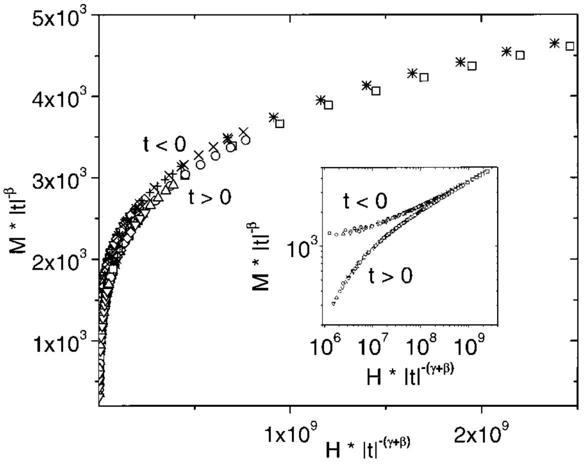

FIG. 8. Scaling plot of M/t^{β} vs $H/t^{(\beta+\gamma)}$ with β, γ, δ, and T_C values from Figs. 5–7. Different symbols represent different temperatures. Linear plot emphasizes the difference in high H, whereas log plot emphasizes the difference in low H.

satisfied within experimental error. The second relation $\gamma-\beta(\delta-1)=0$ (theory), 0.02 ± 0.07 (experiment) is very well satisfied.

IV. DISCUSSION

The critical exponents for this experiment and theoretical values for mean field, 3D Heisenberg, 3D *XY*, 3D Ising model are listed in Table I. The critical exponents α, β, γ, and δ obtained in the present experiment are all between 3D-Ising-model and mean-field values. The values we find are completely consistent with those reported by Ghosh *et al.* on a single-crystal sample, and significantly different than those found by Mohan *et al.* The mean-field-like values found by Mohan *et al.* suggested that long-range coupling could be important in the manganites; the values found here and by Ghosh *et al.* suggest that shorter-range coupling is a better model. The deviations from 3D Heisenberg could be due to uniaxial anisotropy causing a crossover effect to the 3D Ising model with the final critical behavior visible only at still lower reduced temperatures. We estimated the temperature range at which crossover occurs from the 3D Heisenberg model to the 3D *XY* model. The criterion for this crossover temperature was $K_H\,\xi^3\sim k_B T_C$, i.e., the hard-axis anisotropy energy within the correlated volume is on the order of the thermal energy. $\xi=\xi_0|t|^{-v}$, where the correlation-length exponent $v=(2-\alpha)/d=0.65$ is predicted by an exponent relation with the experimental value for $\alpha=0.05$. The shape-anisotropy energy at reduced temperature t, $K_H(t)=K_H$ (300 K) $M_S^2(t)/M_S^2$(300 K) was calculated using the spontaneous magnetization from the experiment. We assumed the zero-temperature correlation length $\xi_0\sim5$ Å, from the neutron scattering data of the same sample.[11] The error in $\xi_0=5\sim10$ Å is not as important as the error in v. We did not use their value of $v=0.4$ because this value of v yields $\alpha=0.8$, too large compared to our experiment. As a result, we get $t_{x1}\sim0.02$ for the crossover from 3D Heisenberg to 3D *XY*. Likewise, the crossover from 3D *XY* to 3D Ising was estimated as $t_{x2}\sim0.004$ by using $K_E=4.1\times10^4$ dyne/cm^2 instead of K_H. t_{x1} is within the experimental temperature range for critical exponent α. t_{x2} is within the experimental temperature range for critical exponents α and γ (see Table I). Therefore the anisotropy plays a big role in the critical analysis and we do not expect to see pure 3D Heisenberg behavior within our experimental temperature range. Furthermore, the amplitude ratio A/A' in Table I is closer to the 3D Ising (or 3D *XY*) model than the 3D Heisenberg model. All our results point towards the 3D Ising model rather than the 3D Heisenberg model.

There are many similarities between manganites and high-T_C superconductors. The short correlation length is an example. In the high-T_C superconductors, there was an analysis of crossover effects on the heat capacity of YBa$_2$Cu$_3$O$_{7-x}$ from the mean-field to the 3D *XY* model.[21] They estimated the temperature at which the fluctuation contribution to C_P becomes as significant as the mean field. This Ginzburg criterion, $t_G=(1/32\pi^2)(k_B/\Delta C\xi_0^3)^2$ was estimated to be of the order of 10^{-3}, using $\xi_0=10$ Å. If this is also the case with LSMO, then we can expect the crossover from the mean-field to 3D Ising model since t_G is of the same order as t_x above. Our results are consistent with this analysis. In other words, the temperature region suitably describable by 3D Heisenberg model can be estimated as $t_G<t<t_x$. Because t_G is of the same order as t_x due to the short correlation length and large anisotropy, essentially we see a crossover from the mean-field model directly to the 3D Ising model, skipping 3D Heisenberg. In this view, the mean-field behavior reported by Mohan *et al.* can also be understood. If we assume that the average crystallite size of their polycrystalline sample is 500 Å, then as the temperature gets closer to T_C, at $t\sim0.001$ the correlation length, $\xi=\xi_0|t|^{-v}$, would exceed the grain size, therefore the fluctuation effects will be replaced by mean-field behavior again. Assuming the domain size of our single-crystal sample is 5 μm as observed by SEM,[11] we have to get to $t\sim10^{-6}$ to observe similar effects. Since our reduced-temperature range is larger than this, fluctuation effects are still important for the single-crystal sample.

V. CONCLUSIONS

We have made magnetization and specific-heat measurements on a small (sub-mg) single crystal of La$_{0.75}$Sr$_{0.25}$MnO$_3$. From the specific heat above 400 K, all phonon modes appear to be excited, implying Debye and Einstein temperatures of less than 400 K. The phase transition is very sharp, suggesting the homogeneity of the sample with no phase separation. Good homogeneity was possible partly due to the small size of the sample we looked at. The critical exponent α was found to be $+0.05\pm0.07$. At low temperatures, the saturation magnetization reached the spin-only value of $3.75\mu_B$, indicating no canting of the spins. Critical exponents derived from modified Arrot plots $\beta=0.40\pm0.02$, $\gamma=1.27\pm0.06$, and $\delta=4.12\pm0.2$ are consistent with the equalities expected from the scaling hypothesis, also supporting a second-order phase transition in this material. All critical exponent values are between the mean-field and 3D Ising model. The 3D Ising model is more relevant than 3D Heisenberg due to anisotropy. Fluctuations are important when crystallite and magnetic domain sizes are large. Further studies of the crossover analysis will be useful to confirm this view. Although no simple model explanation is possible, the exponent relations are well satisfied.

ACKNOWLEDGMENTS

We would like to thank M. Salamon and R. Fisch for their insights and discussions on the critical-exponent theory, M. Viret and E. N. Abarra for their help with the experiments, and the NSF for support. We thank Alex Revcolevschii for kindly providing the crystals used in the experiment.

---

[1] S. Jin, T. H. Tiefel, M. McCormack, R. A. Fastnacht, R. Ramesh, and L. H. Chen, Science **264**, 413 (1994); R. von Helmolt, J. Wecker, B. Holzapfel, L. Schultz, and K. Samwer, Phys. Rev. Lett. **71**, 2331 (1993); K. Chahara, T. Ohno, M. Kasai, and Y. Kozono, Appl. Phys. Lett. **63**, 1990 (1993); R. M. Kusters, J. Singleton, D. A. Keen, R. McGreevy, and W. Hayes, Physica (Amsterdam) **155B**, 362 (1989).

[2] See, for example, review articles by A. Ramirez, J. Phys.: Condens. Matter **9**, 8171 (1997); J. M. D. Coey, M. Viret, and S. von Molnar, Adv. Phys. **48**, 167 (1999).

[3] K. Ghosh, C. J. Lobb, R. L. Greene, S. G. Karabashev, D. A. Shulyatev, A. A. Arsenov, and Y. Mukovskii, Phys. Rev. Lett. **81**, 4740 (1998).

[4] J. M. D. Coey, M. Viret, L. Ranno, and K. Ounadjela, Phys. Rev. Lett. **75**, 3910 (1995).

[5] S. Yunoki, J. Hu, A. L. Malvezzi, A. Moreo, N. Furukawa, and E. Dagotto, Phys. Rev. Lett. **80**, 845 (1998); G. Papavassiliou, M. Belesi, T. G. Maris, G. Kallias, M. Pissas, D. Niarchos, C. Dimitropoulos, and J. Dolinsek, *ibid.* **84**, 761 (2000); M. Uehara, S. Mori, C. H. Chen, and S.-W. Cheong, Nature (London) **399**, 560 (1999).

[6] J. Lynn, R. W. Erwin, J. A. Borchers, Q. Huang, and A. Santoro, Phys. Rev. Lett. **76**, 4046 (1996); P. Lin, S. H. Chun, M. B. Salamon, Y. Tomioka, and Y. Tokura, J. Appl. Phys. **87**, 5825 (2000).

[7] S. E. Lofland, V. Ray, P. H. Kim, S. M. Bhagat, M. A. Manheimer, and S. D. Tyagi, Phys. Rev. B **55**, 2749 (1997).

[8] P. Lin, S. H. Chun, M. B. Salamon, Y. Tomioka, and Y. Tokura, J. Appl. Phys. **87**, 5825 (2000).

[9] Ch. V. Mohan, M. Seeger, H. Kronmüller, P. Murugaraj, and J. Maier, J. Magn. Magn. Mater. **183**, 348 (1998).

[10] M. C. Martin, G. Shirane, Y. Endoh, K. Hirota, Y. Moritomo, and Y. Tokura, Phys. Rev. B **53**, 14 285 (1996).

[11] M. Viret, H. Glättli, C. Fermon, A. M. De Leon-Guevara, and A. Revcolevschi, Europhys. Lett. **42**, 301 (1998).

[12] D. W. Denlinger, E. N. Abarra, K. Allen, P. W. Rooney, M. T. Messer, S. K. Watson, and F. Hellman, Rev. Sci. Instrum. **65**, 946 (1994).

[13] E. O. Wollan and W. C. Koehler, Phys. Rev. **100**, 545 (1955).

[14] B. F. Woodfield, M. L. Wilson, and J. M. Byers, Phys. Rev. Lett. **78**, 3201 (1997).

[15] A. M. Kadomtseva, Yu. F. Popov, K. I. Kamilov, G. P. Vorobev, A. A. Mukhin, V. Yu. Ivanov, and A. M. Balbashov, Physica B **284–288**, 1410 (2000).

[16] Chang Fanggau, M. Cankurtaran, G. A. Saunders, A. Al-Kheffaji, D. P. Almond, P. J. Ford, and D. A. Ladds, Phys. Rev. B **43**, 5526 (1991).

[17] The dilation contribution $C_P - C_V = V_m \beta^2 T/K_T$, where the molar volume $V_m = 35\,\mathrm{cm}^3/\mathrm{mol}$ (see Ref. 10) volume thermal-expansion coefficient, $\beta = 3\alpha = \sim 1.6\times 10^{-5}\,\mathrm{K}^{-1}$, $K_T = 1/B_0$ (B_0 is the bulk modulus) $\sim 1.1\times 10^{-12}\,\mathrm{cm}^2/\mathrm{dyne}$ is the isothermal compressibility estimated from the value for $La_{1.8}Sr_{0.2}CuO_4$ because B_0 is not available for LSMO, see, e.g., F. Reif, *Fundamentals of Statistical and Thermal Physics* (McGraw-Hill, New York, 1965), p. 168.

[18] A. Kornblit and G. Ahlers, Phys. Rev. B **11**, 2683 (1975).

[19] See, for example, Philip R. Bevington and D. Keith Robinson, *Data Reduction and Error Analysis for the Physical Sciences* (McGraw-Hill, New York, 1992).

[20] S. N. Kaul, J. Magn. Magn. Mater. **53**, 5 (1985).

[21] George Mozurkewich, M. B. Salamon, and S. E. Inderhees, Phys. Rev. B **46**, 11 914 (1992).